Available online at www.sciencedirect.com
SCIENCE DIRECT®
ELSEVIER
Earth and Planetary Science Letters xx (2006) xxx–xxx
EPSL
www.elsevier.com/locate/epsl

Holocene slip-rate on the Sabzevar thrust fault, NE Iran, determined using optically stimulated luminescence (OSL)

Morteza Fattahi [a,b,c,*], Richard Walker [c], James Hollingsworth [d], Abbas Bahroudi [e], Hamid Nazari [e], Morteza Talebian [e], Simon Armitage [b], Stephen Stokes [b]

[a] *The Institute of Geophysics, Tehran University, Kargar Shomali, Tehran, Iran*
[b] *School of Geography, Oxford University Center for the Environment, South parks Road, Oxford OX1 3QY, United Kingdom*
[c] *COMET, Department of Earth Sciences, University of Oxford, Parks Road, Oxford, OX1 3PR, United Kingdom*
[d] *COMET, Bullard Laboratories, Madingley Road, Cambridge, CB3 0EZ, United Kingdom*
[e] *Geological survey of Iran, Azadi square, Tehran, Iran*

Received 22 June 2005; received in revised form 9 December 2005; accepted 18 March 2006

Editor: R.D. van der Hilst

Abstract

Fault slip-rates and the recurrence interval between earthquakes can be determined from reliable dating of deformed sediments. We report optically stimulated luminescence (OSL) ages of alluvial gravels, fine-grained sediments and colluvial deposits associated with the Sabzevar thrust fault in northeastern Iran. Six samples of the late Quaternary deposits were dated by OSL using the single aliquot regenerative-dose (SAR) protocol. The OSL ages indicate deposition of alluvial gravels in the study region between ~30 and ~9–13 ka, followed by a period of fluvial incision which is ongoing at the present day. The alluvial deposits have been uplifted by ~9.5 m relative to the river level, indicating a Holocene slip-rate of ~1 mm/yr and a rate of convergence across the fault of 0.4–0.6 mm/yr assuming a maximum fault dip of 60°. The average interval between large earthquakes on the Sabzevar fault will be ~3000 years if the fault dips ~60°, and less if the fault dip is less. The last earthquake to destroy Sabzevar was in 1052 A.D.

Keywords: luminescence dating; fault slip-rate; Iran; earthquake; seismic hazard

1. Introduction

Active faults in Iran pose a serious hazard for a large percentage of the population and earthquakes often cause deaths into the tens of thousands. For instance, the Mw 7.4 Tabas event in 1978 caused over 20,000 deaths [1], the 1990 Rudbar-Tarom earthquake killed at least 30,000 [2], and more recently, a Mw 6.5 earthquake on the 26th December 2003 resulted in the loss of over 30,000 lives and the almost total destruction of the ancient city of Bam and surrounding villages (e.g. [3]).

Very little is known of slip-rates, and therefore of the average intervals between earthquakes, on faults in Iran-information which is vital for estimates of seismic hazard. The repeat time between earthquakes on individual active faults is typically rather long (>1000 years), and

* Corresponding author. COMET, Department of Earth Sciences, University of Oxford, Parks Road, Oxford, OX1 3PR, United Kingdom. Fax: +44 98 21 8009560, +44 1865271929.
E-mail addresses: mfattahi@ut.ac.ir, morteza.fattahi@ouce.ox.ac.uk (M. Fattahi).

0012-821X/$ - see front matter © 2006 Elsevier B.V. All rights reserved.
doi:10.1016/j.epsl.2006.03.027

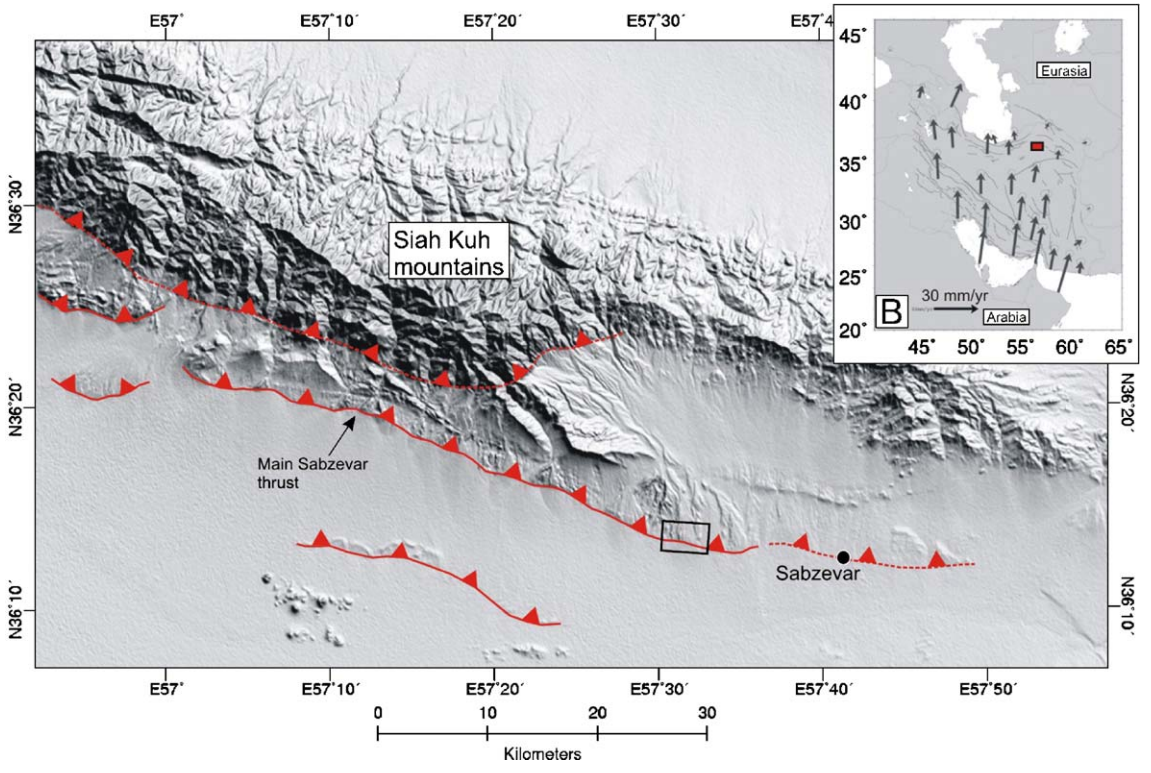

Fig. 1. 90 m SRTM (Shuttle-borne Radar Topography Mission) topography of the Sabzevar region and Siah Kuh mountain range. Major active faults are marked with solid black toothed lines (red in on-line version). The main segment of the Sabzevar thrust extends for at least ~60 km across most of the image, and may continue as far east as Sabzevar city. The box shows the location of Fig. 2. (Inset) The location of the figure within Iran is represented by the white box (red in on-line version). GPS velocities of points relative to Eurasia are shown [7].

the historical record, although excellent (e.g. [4], is too short to fully determine the earthquake hazard in a given region (e.g. [5]). In order to determine the average interval between earthquake events we must therefore determine the history of slip on individual faults over timescales of several thousands, or tens of thousands, of years. At present, analytical Quaternary dating techniques have been applied in only one study of active faulting in the interior of Iran, where two generations of young alluvial fans displaced by the Minab-Zendan fault system in SE Iran, have been dated at 5–9 and ~13 ka [6].

In this study we report optically stimulated luminescence (OSL) ages of sediment samples from alluvial, fine-grained infill and colluvial deposits deformed by movements on the Sabzevar thrust fault in northeast Iran. The OSL analyses for both alluvial and wind-blown material give consistent ages, and suggest to us, at least in this example, that OSL dating has applicability in dating alluvial deposits. This is especially important in arid regions such as Iran, where fine-grained deposits are uncommon, and organic matter for C^{14} dating is rarely found in sediments.

Our results allow us to estimate the Holocene slip-rate on the Sabzevar thrust. The fault in our study region is known to be seismically active, and the city of Sabzevar (with a population of ~200,000) was destroyed by an earthquake in 1052 A.D. (e.g. [4]). The youngest evidence of surface faulting identified at our site is dated at $<3\pm0.3$ ka and may represent deformation from this event.

2. Geological and tectonic background

The active tectonics of Iran is dominated by the northward motion of Arabia with respect to Eurasia (Fig. 1 inset). At longitude 56E, ~25 mm/yr of north–south shortening is accommodated across Iran (e.g. [7]). Shortening is accommodated by a combination of thrust and strike-slip faulting in seismically active parts of both southern and northern Iran. The northward-dipping Sabzevar thrust fault is situated along the southern margin of the east–west trending Siah Kuh (Black Mountain) range in northeast Iran (Fig. 1). The Siah Kuh mountains expose a sequence of Cretaceous and Mid-Tertiary (Eocene) ophiolitic and volcanic rocks [8].

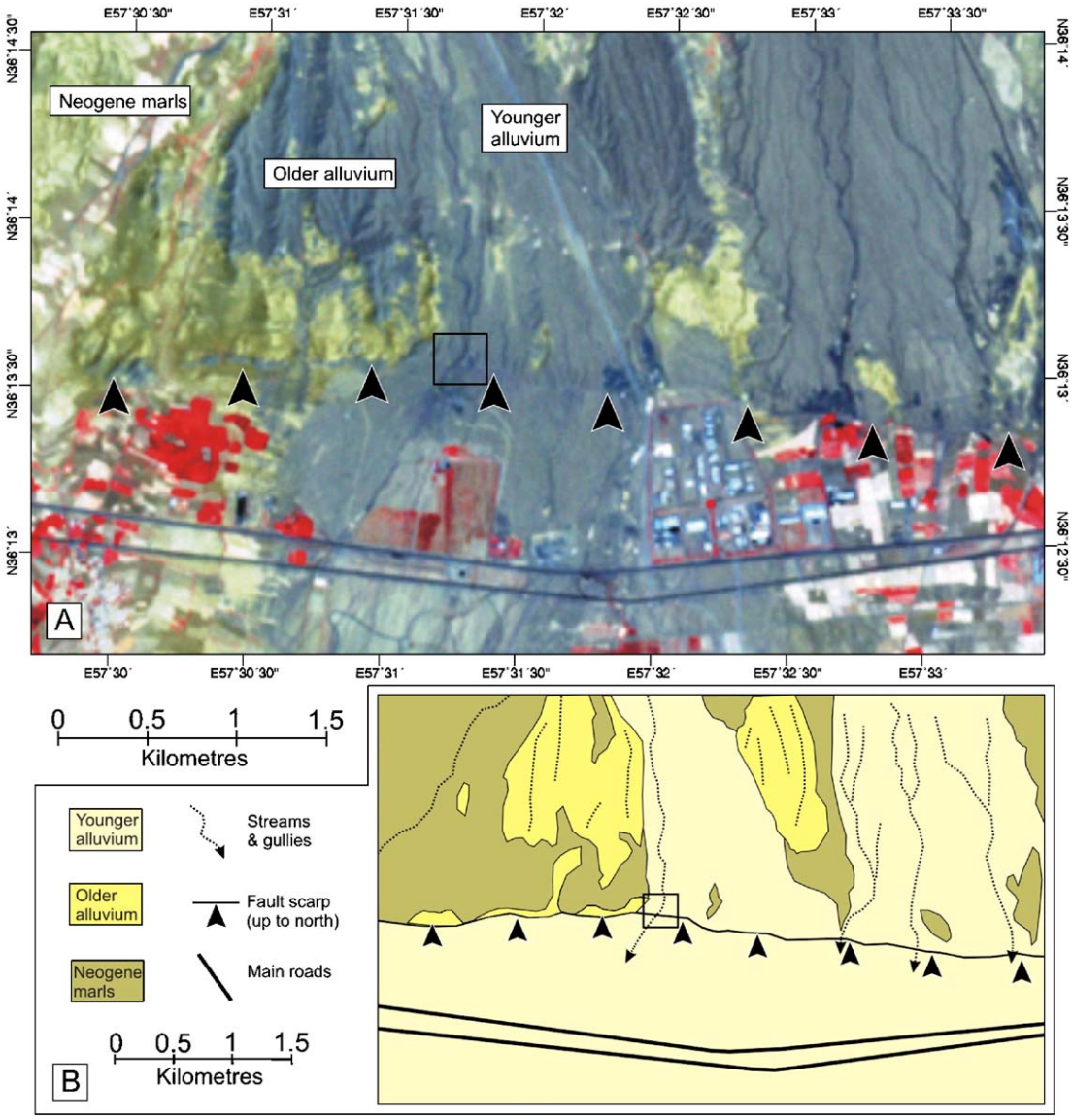

Fig. 2. (A) ASTER satellite image of the sampling site (boxed region) and surrounding parts of the Sabzevar fault scarp (marked by black arrows). Areas to the north of the scarp have been uplifted. Several generations of gravel fan deposits cross the fault. Older fans surfaces are now higher above the present-day river level and are more dissected than younger fans. Our samples were taken from the lowest, and therefore youngest, generation of alluvial fan. The alluvial deposits overlie Miocene marls (light coloured in the satellite image), which outcrop at several places on the uplifted side of the fault. (B) Geomorphic map of the study region, highlighting the generations of gravel fan deposits and exposures of underlying Miocene marls.

Miocene red marls are exposed on the upthrown side of the Sabzevar fault. The marls are covered in a number of areas by Quaternary fluvial and alluvial gravels.

There has been little instrumental seismicity in the Sabzevar region (Fig. 1), although the town was slightly damaged by earthquakes on the 12th December (Mb 4.2) and 17th December 2004 (Mb 3.4), which had epicentres of 35.95N 57.95E and 36.35N 58.31E respectively (epicentres and magnitudes are from the USGS-NEIC PDE catalogue). Historical records reference a major earthquake in 1052 A.D. (named the Baihaq earthquake [4]). This earthquake, and strong aftershocks over the following month, reduced the city of Sabzevar to ruins. The event was felt over a wide area, but the distribution of damage is not known and no surface ruptures were recorded [4]. As the Sabzevar thrust is the major identifiable active fault in the region, and passes very close to the city (Fig. 1), it seems likely, though not certain, that it was responsible for the 1052 A.D. earthquake. The Sabzevar fault is at least 60 km

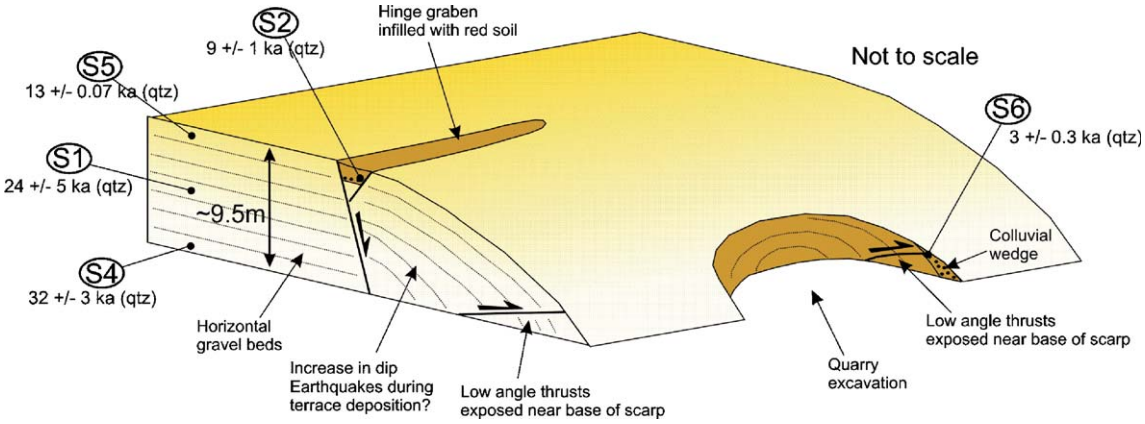

Fig. 3. Block diagram showing the major features of the sampling site and results of the OSL analyses. Sections through the 9.5 m high scarp were provided by a river cutting (along the near side of the block diagram, see Fig. 5) and by a small quarry excavation. Bedding in gravels within the scarp steepen downwards, implying uplift and growth during deposition of the terrace. The scarp is cut by a hinge graben infilled with windblown sediment, and by low angle thrusts at the base of the scarp.

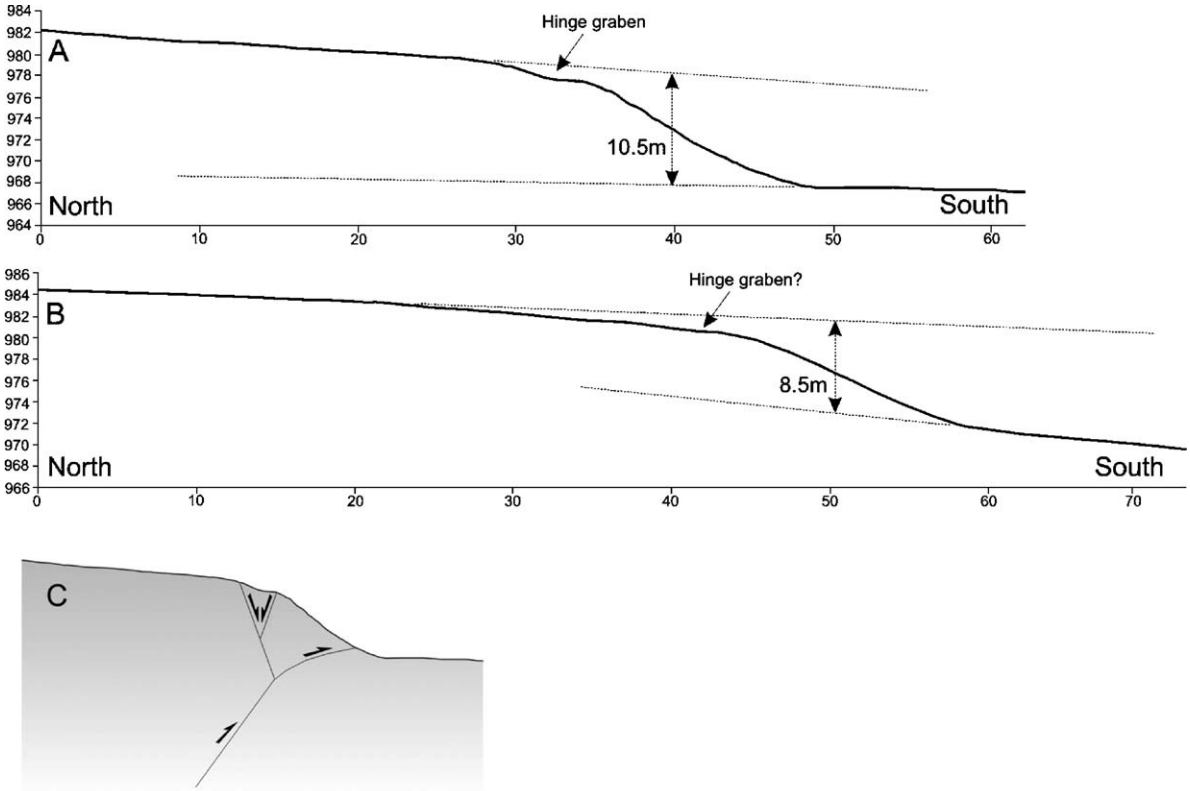

Fig. 4. (A) and (B) Differential GPS profiles taken perpendicular to the trend of the scarp. The amount of deformation of the top surface of the gravels across the scarp is 10.5 m (+/−0.1 m) in profile (A), which was taken at the sampling site, and 8.5 m (+/−0.1 m) in profile (B), which was taken a few tens of metres to the east. The hinge graben appears as a slight depression in the top surface of the terrace. The height of the terrace at the hinge graben is ~7 m (compare with Fig. 5). (C) Sketch of inferred faulting at depth (adapted from [9]). The hinge graben is likely to result from a near-surface flattening of the fault plane. The dip of the seismogenic Sabzevar thrust may thus be up to 60°.

long and could generate magnitude 7 earthquakes. One of the major aims of our project is to provide a time-averaged rate of slip for the Sabzevar fault, in order to estimate the likely recurrence interval between earthquakes, assuming that the fault fails in events with M7.

3. Site description and sampling methods

We focus on one site along the Sabzevar fault at 36:13:18N 57:31:33E (Fig. 2), where a scarp in alluvial gravels has been incised by a southward flowing river and also partly excavated by gravel quarrying, providing two closely spaced cross-sections through the fault (Figs. 2 and 3). Sediments in the alluvial terrace are composed of coarse, and generally poorly cemented, gravels. The top ~20 cm of the gravel beds have been altered to a red soil. The gravels are sourced from the Siah Kuh mountains to the north and clasts are generally rich in quartz and feldspars. The terrace deposits overlie regionally extensive Miocene marls.

North–south topographic profiles perpendicular to the scarp show a gradual northward increase in the gradient of the top surface of the terrace (Fig. 4). The mean height change of the terrace across the scarp is ~9.5 m (measured from two differential GPS profiles in Fig. 4). North of the scarp, the terrace surface has roughly the same gradient as the alluvial surface south of the scarp. As river incision stops close to the base of the scarp, we can assume that the ~9.5 m of terrace deformation is caused by fault uplift rather than a regional lowering of the river bed. Gravel beds exposed in the river cutting show similar attitudes to the top of the terrace, with roughly horizontal beds in the north steepening rapidly at the scarp (Fig. 5). Within the scarp, the southward dip of lower gravel beds (>10°) is significantly greater than the dip of upper layers (~5°). This growth suggests that uplift, presumably during earthquakes, occurred during deposition of the terrace (Fig. 5). The top surface of the abandoned terrace can only be used as a marker of post-depositional fault movement if it was originally laid down as a flat layer. However, as fault uplift has occurred during deposition of the alluvial gravels, the successive alluvial layers may have draped over a folded surface, in which case the ~9.5 m of terrace deformation will be an overestimate of the true amount of movement since abandonment of the terrace. The change in dip between upper and lower gravel units within the scarp is too small to determine with certainty whether individual beds show growth, which is likely if the beds were draped over a folded surface, or whether the beds are separated by minor unconformities. At least in the upper 1–2 m of the sequence we see no evidence of growth within individual beds (e.g. Fig. 5), suggesting that the terrace was deposited as a flat surface and is a valid marker of deformation.

The scarp is cut by two zones of faulting. Near the top of the scarp, southward- and northward-dipping normal faults (both dipping ~70°) have opened up a small graben (~4 m wide) in the gravel beds (Fig. 5). The southward-dipping fault is dominant. The graben infill is composed of ~70 cm of red fine-grained soil, containing a few coarse clasts, which overlie the coarse gravel beds at the base of the graben. It appears that this infill is predominantly wind-blown or possibly derived

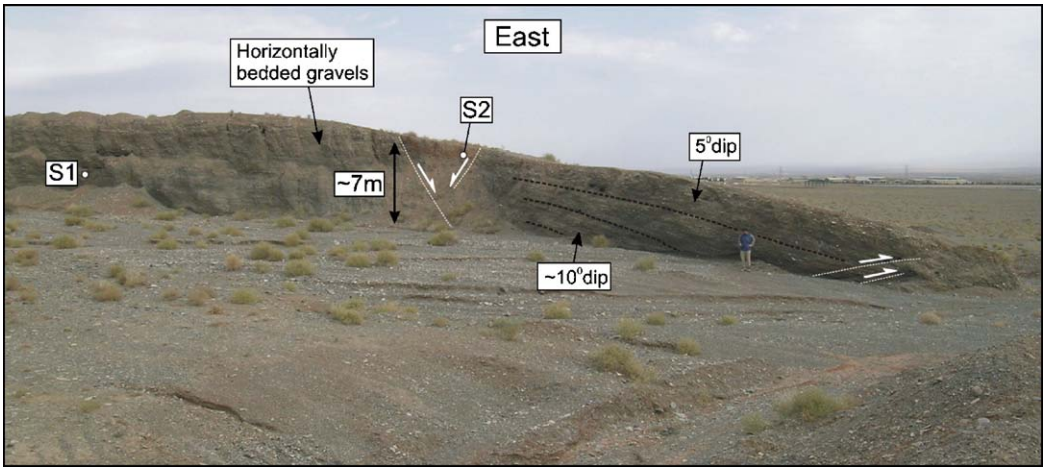

Fig. 5. Photograph looking east from 36:13:21.1N 57:31:29.5E at the Sabzevar fault scarp exposed in a river cutting. Compare with the block diagram in Fig. 3. Sample location S1 and S2 are shown. Sample S4 was collected from further north, out of the frame of the image. Sample S5 was collected from a pit dug into the top surface of the terrace. Figure for scale.

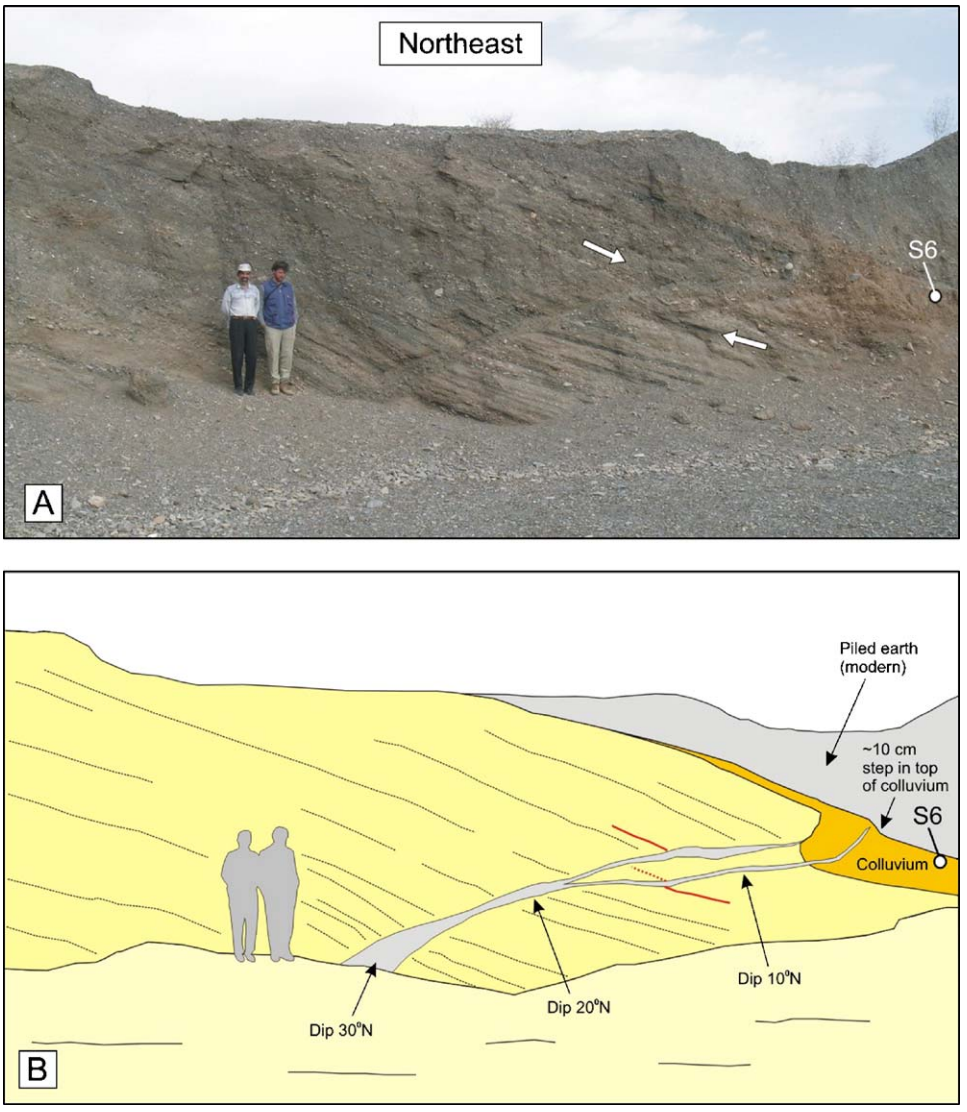

Fig. 6. Photograph looking northeast at thrust faults in the wall of a quarry excavation. The fault zone narrows and decreases in dip towards the surface, eventually splitting into two strands. The total displacement across the faults is ~50 cm (a displaced bed is marked as a white line (red in on-line version), see Fig. 7). The lower strand cuts the top of a wedge of colluvial deposits creating an ~10 cm step. The S6 sampling site is shown.

from low energy surface run-off. On the top surface of the terrace, the graben can be traced as a shallow depression with a concentration of shrubby vegetation. The graben is ~5–10 m long, it is parallel to the trend of the scarp and there is no evidence of a lateral component of motion in the form of en-echelon stepping.

At the base of the scarp, at least two low angle thrust faults are observed (Figs. 5 and 6). In the quarry exposure, the fault zone appears to narrow towards the surface, with a roughly 20 cm wide zone of imbricated and cemented gravels at the base of the exposure narrowing into a 10 cm wide zone, which eventually breaks into two separate strands near the surface (Fig. 6). The lower strand appears to be the youngest, and the top surface of a wedge of red colluvium associated with the upper strand has been displaced by ~10 cm by the lower fault (Figs. 6 and 7). The total displacement across the two thrust faults exposed in the near-surface sediments is ~50 cm (Fig. 7), suggesting that only a small amount of the slip at depth responsible for the ~9.5 m of uplift reaches the surface on them, with the remainder presumably accommodated as folding in the scarp, or possibly as slip on other faults which are not exposed in the cutting.

The thrust faults strike at 150°, slightly oblique to the overall trend of the fault (Fig. 2). In the quarry exposure, the observed dips decrease towards the surface from ~30°

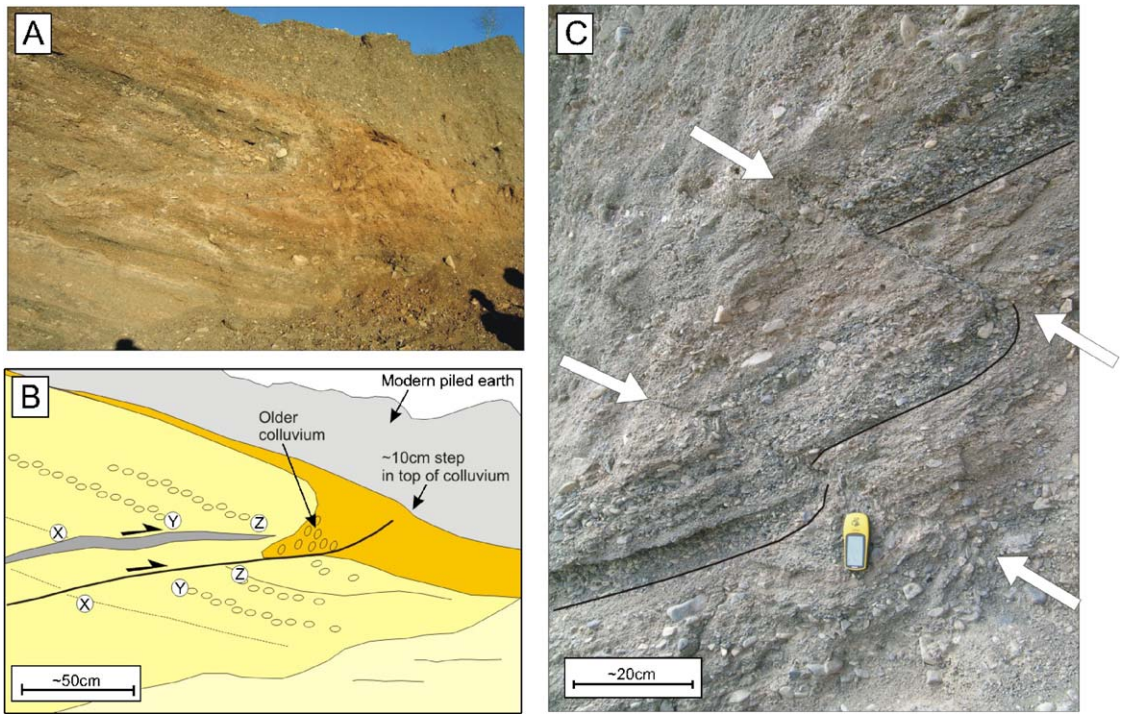

Fig. 7. (A) Photograph looking east from 36:13:19.7N 57:31:33.0E at the deformed colluvial wedge deposits in the east wall of the quarry exposure. (B) Sketch of the photograph in (A). Two fault strands cut through gravel beds. The total displacement across the faults is ~50 cm (displaced beds X, Y and Z are highlighted). The lower fault strand has a total displacement of ~10–15 cm and cuts through the top of the colluvial sediments. Lower parts of the wedge are substantially deformed by faulting and may represent older deposition. (C) View looking west at the two fault strands in the west wall of the quarry exposure. A distinctive gravel band shows the displacements of ~10–15 and ~35 cm across the two strands. GPS receiver for scale.

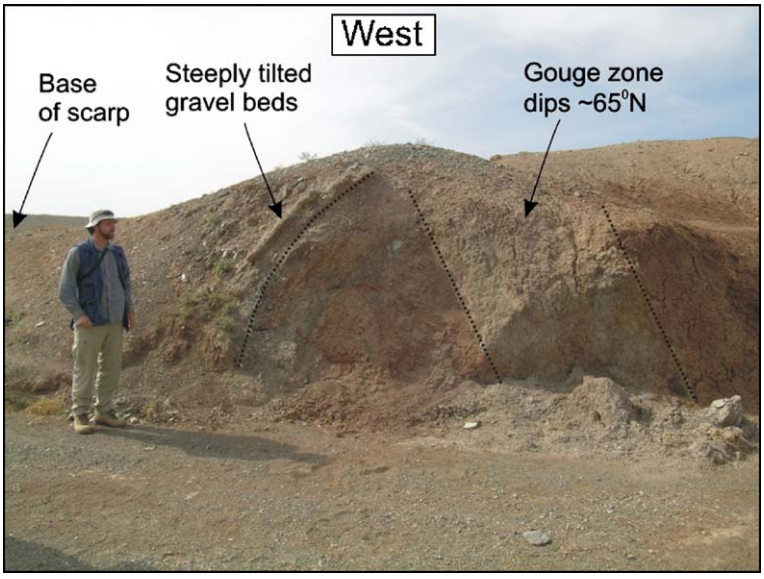

Fig. 8. View west from 36:14:20.9N 57:27:49.7E of fault exposure at the base of the Sabzevar scarp. A 2 m wide gouge zone dips ~60° to the N. Overlying gravel beds are steeply tilted, and increase in dip from 40° S to 80° south over ~2 m horizontal distance.

Table 1
Generalized single aliquot regenerated sequence (refer to Section 4 for details)

Step	Treatment	Observed
1	Give dose	–
2	Pre-heat	–
3	Stimulation	L_x
4	Give test dose	–
5	Pre-heat	–
6	Stimulation	T_x
7	Return to 1	–

Note: In steps 2 and 5, the sample has been heated to the pre-heat temperature using *TL* and held at that temperature for 10 s.
$N = L_0/T_0 = L_n/T_n$; $R_x = L_x/T_x$ (x=1,5).

N to ~10° N (Fig. 6). Near surface decreases in fault dip have been described in many examples of thrust faulting (e.g. [9–11]). Bending and collapse of the scarp often lead to the formation of hinge grabens (e.g. Fig. 4). It is therefore likely that the seismogenic Sabzevar fault is much steeper than the maximum 30° observed at the sample site (e.g. Fig. 4C). This is supported by a fault exposure at 36:14:20.9N 57:09:19.4E, where a 2 m thick gouge zone dips ~60–65° to the north (Fig. 8).

We collected 6 samples for OSL dating (locations are shown schematically on Fig. 3). Our samples were selected to provide the maximum amount of information on the duration of sediment aggradation, the abandonment of the alluvial terrace, and the subsequent fluvial incision of the terrace deposits as a result of fault uplift. We also took samples from colluvial sediments cut by faulting and from the infill of the small fault-controlled graben in order to provide bounds on the recent history of earthquakes.

The samples were collected by either inserting plastic tubes (5 cm diameter by 25 cm long) into the deposit (samples S2, S3 and S6); by taking a block of sediment trimmed in the dark (samples S1 and S4); or by collecting a bag of loose sediment whilst protected from the light by coverings of black plastic and canvas blankets (sample S5). Dose rates were measured in situ with a micro-nomad portable spectrometer.

4. Luminescence dating

Optically stimulated luminescence (OSL) is the luminescence emitted on illumination due to the release of stored energy accumulated in crystalline materials through the action of ionising radiation from natural radioactivity. This method dates the last sunlight exposure event for mineral grains in the sediment. When sediment is exposed to sunlight prior to deposition, the OSL acquired over geological time is removed. The luminescence "clock" is thus set to zero. After burial the OSL accumulates in response to natural ionising radiation (from radioactive isotopes in the TH, U series and ^{40}K, and from cosmic rays), received during the burial period of the sediment. Quartz and feldspar in the sediment have dosimetric properties. The level of OSL observed in these minerals is thus dependent on the absorbed radiation dose. For age determination two values are required: the equivalent dose D_e (which is the radiation level responsible for producing the luminescence signal) and the dose received per year (during burial).

4.1. Experimental condition

All the experiments reported here were carried out using a Risø (Model TL/OSL-DA-15) automated TL/OSL system (fitted with a ^{90}Sr/^{90}Y beta source delivering ~5 Gy min^{-1}) equipped with an IR laser diode (λ=830 nm) and a blue (λ=470 nm) diode array (p=24 mW cm^{-2}) as stimulation sources. The intensity of laser light incident on the sample was about 400 mW cm^{-2} [12]. OSL was detected using an Electron Tubes bialkaline PMT. Luminescence was measured through 7 mm Hoya U-340 filters.

The sample was processed under subdued red light. The potentially light exposed sediments at both ends of the plastic tubes and around the blocks were extracted, and the sediment remaining was used for equivalent dose determination. A portion of the sample was wet-sieved to separate the fine quartz (38–63 μm) size fractions and immersed for two days in 1 N HCl to remove carbonate, followed by two days immersion in H_2O_2 to remove organic material. The grains in the range of 38–63 μm were treated with 35% Fluorosilicic acid for 2 weeks in order to remove feldspar, followed by 1 h immersion in

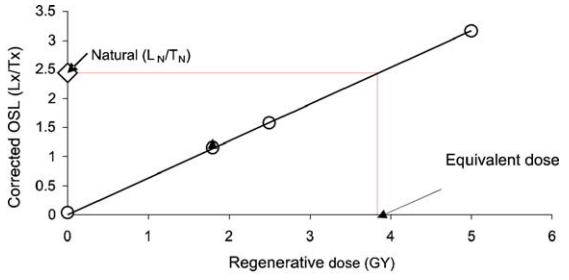

Fig. 9. An example of equivalent dose (D_e) determination for sample S6. Four regeneration doses (L_x, x=1,2,3,4) are given and the sensitivity changes of regenerated OSL data are corrected by dividing the regeneration dose by the subsequent OSL test dose response (T_x, x=1,2,3,4). The ratios (L_x/T_x, x=1,2,3,4) are demonstrated as open circles. A linear fit is applied to the regenerated data points. The sensitivity corrected natural OSL response (L_n/T_n) is marked. The equivalent dose (D_e) corresponding to the natural OSL response is then read from regenerative dose axis.

1 N HCl. Some aliquots of the separated quartz were tested for feldspar contamination using IRSL, following bleaching the sample by IR and running one stage of SAR method (Table 1). After several treatments with acids, the samples were effectively pure quartz and then processed for equivalent dose measurement. A second stage of dry sieving through a 38 μm sieve was undertaken to obtain the final quartz concentrate used for the experiments. The quartz separates were mounted as a monolayer (approximately 5 mg/disc) on 10 mm diameter aluminium discs using a silicon spray as an adhesive.

4.2. D_e determination

Over the last few years single aliquot protocols have been used to measure equivalent doses (D_e) in quartz and feldspar luminescence dating (e.g., [13–17]. Both additive dose and regenerative dose approaches have been employed. As regenerative methods interpolate the natural luminescence signal onto a growth curve, in doing so estimating D_e independent of growth curve model (e.g., [18]), they offer intrinsic advantages over additive dose approaches. Regeneration methods have, however, been complicated by the widespread occurrence of sensitivity changes in both quartz (e.g., [19]) and feldspar (e.g., [20,21]).

Murray and Wintle [13] developed a single aliquot regeneration (SAR) protocol for quartz which explicitly tests and corrects for sensitivity changes which is rapidly becoming the standard procedure for D_e determination for that dosimeter. The SAR procedure (Table 1) critically depends on the assumption that it is possible to measure a signal after each dose and stimulation cycle which acts as a surrogate measure of the sensitivity of the aliquot during the preceding measurement cycle. As such, any sensitivity changes which have occurred in the course of a regenerative analysis can be corrected, for both the natural and regenerated signals.

In this study the equivalent dose (D_e) was obtained using the single aliquot regeneration method (Table 1) for quartz. Laboratory beta dose rate was applied

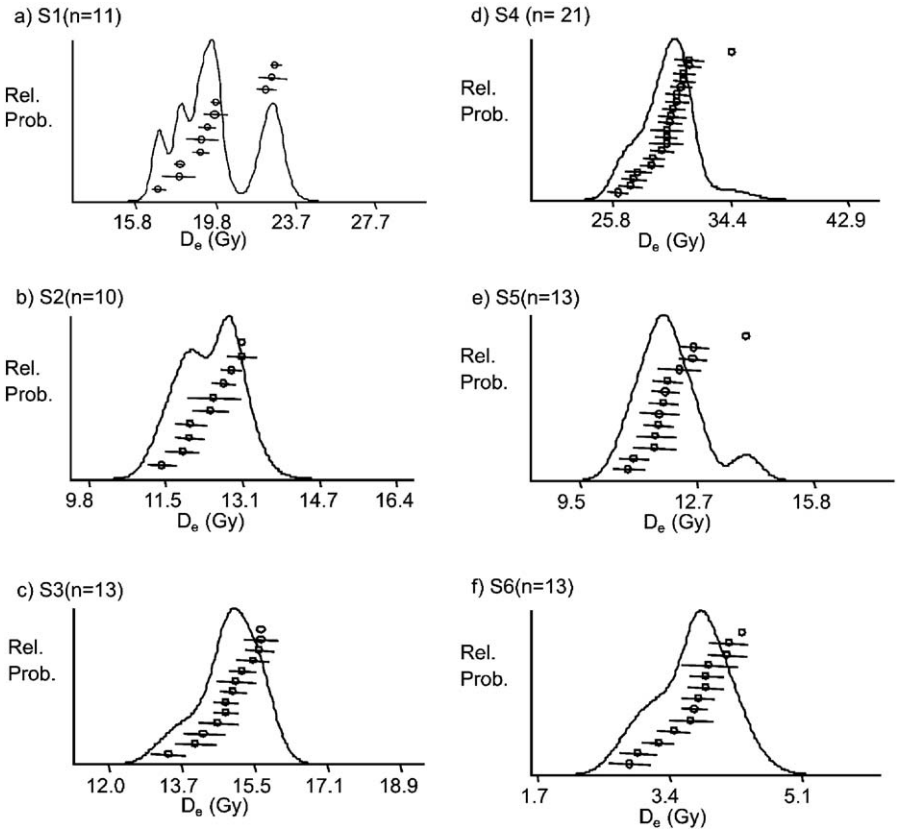

Fig. 10. Equivalent dose distribution diagrams from SAR OSL for Sabzevar quartz samples. The tightly defined peaks in equivalent dose measured for samples S2 to S6 indicate resetting of the OSL signal on deposition, and as such, suggest that the calculated OSL ages are close to the true deposition ages. Plots were produced using the Analyst software written by G. Duller (Pers. Comm.).

Table 2
Values used to calculate luminescence ages from Sabzevar fault, NE Iran

Sample	Equivalent dose [a]	Dose rate [b]	Age
	(Gy)	(mGy/yr)	(ka)
S1	19.3±4.5	0.81±0.04	24±5
S2	12.43±1.07	1.39±0.04	9±1
S3	14.99±0.55	1.13±0.04	13.3±0.7
S4	28.20±2.22	0.86±0.04	32±3
S5	11.96±0.4	094±0.04	13±0.7
S6	3.71±0.03	1.17±0.04	3±0.3

[a] Des were calculated using quartz (38–63 micron).
[b] Dose rates were calculated using field gamma spectrometry (see text).

according to [22]. The full technical details will be presented elsewhere [23]. The pre-heat and cut heat treatment used for all quartz sub-samples were 260 and 220 °C for 10 s respectively. OSL was measured for 100 s at 125 °C.

At least twelve disks were prepared from each sample and following measurement of the natural dose, a dose–response curve was constructed from five dose points including three regenerative doses, and a zero dose (Fig. 9) A replicate measurement of the lowest regenerative dose was carried out at the end of each SAR cycle. Fig. 10 shows the dose distribution diagrams for all samples.

4.3. Dose rate and age determination

Uranium, thorium and potassium concentrations were measured using field gamma spectrometry. Present-day moisture contents were determined by drying at 40 °C in the laboratory. The conversion factors for water contents of Aitken, [24], were used for the calculation of alpha, beta and gamma dose rates. Alpha and beta dose rates were corrected for attenuation due to grain size using the factors of Bell [25] and Mejdahl [26]. Dose rates and ages for each sample are presented in Table 2.

4.4. Dose distributions and re-setting of the samples

The relationship of our OSL dates to the sediment deposition ages is worth discussing. All but one of our samples are taken from coarse gravel deposits. Sediment grains may not have been exposed sufficiently to sunlight to reset the OSL signal during deposition in relatively high-energy alluvial environments [27,28]. OSL ages from gravel deposits may therefore be greater than the true age of sediment deposition. However, the degree of re-setting can be estimated from the range of equivalent dose obtained from separate aliquots of each sample. Most dose–response curves were fitted using a linear function (Fig. 9). The errors on individual aliquot D_e values were based on photon-counting statistics, curve fitting error and included a 1.0% systematic measurement error. Equivalent dose distributions have been displayed as probability density functions with individual aliquot D_e values superimposed in ranked order. For most of the samples, the aliquots resulted in a tight D_e distribution (as shown in Fig. 10). However, for sample S1, a tight D_e distribution was not obtained, this may have resulted in the large uncertainties on individual equivalent dose estimates (~20%). The relatively narrow (and symmetrical) distribution of D_e for samples S2 to S6 suggests that these samples were almost completely reset, and as such, our derived OSL ages are likely to be close to the true deposition ages. The larger amount of 'scatter' in the measured D_e of sample S1 could be a result of incomplete bleaching prior to burial.

5. Holocene slip and past earthquakes on the Sabzevar fault

The results of the OSL analysis are summarised in Fig. 3. The three samples S4, S1 and S5 provide an estimate of the duration of alluvial deposition. They indicate that at least 9.5 m thickness of coarse-grained alluvial gravels were deposited from ~30 ka (the lowest sample S4 gives OSL ages of 32+/−3 ka), until ~13 ka (sample S5, taken from ~0.7 m below the top terrace surface, yields an OSL age of 13+/−0.07 ka). Sample S3, with an OSL age of ~13 ka, was taken from gravels exposed at the base of a low flood terrace within the modern river channel. It is possible that sample S3 is composed of deposits from the incised terrace which have been re-worked within the modern fluvial system, and which have an OSL age which was not reset to zero on re-deposition. As with sample S3, samples S1, S4 and S5 are all taken from coarse gravel deposits and their OSL ages may also be greater than the true age of sediment deposition, as sediment grains may not be exposed sufficiently to sunlight during deposition in relatively high-energy alluvial environments ([27,28]). We are however confident that the OSL ages determined from the alluvial gravels (at least for sample S5, and possibly for S4 and S5) are close to the true deposition ages due to the tightly defined peaks in the dose distribution diagrams (Fig. 10), the consistent upward decrease in age between the three alluvial sample ages, and also the consistency with the results of sample S2, described below, which is taken from a fine-grained sediment accumulation.

Sample S2 is taken from the bottom of the fine-grained infill of a small graben near the top of the scarp (Figs. 3 and 5) and yields an OSL age of 9 +/− 1 ka (9.5 +/− 1 using the fine-grained poly-mineral fraction). From the absence of coarse-grained sediment, the infill is likely to be wind-blown, or transported by low-energy surface run-off, or a combination of both. Deposition of sediments in environments such as these, where the sediments will have had long exposure to sunlight, is considered to be well suited to OSL methods, and we are confident that the S2 OSL age is close to the true deposition age. In addition, the dose distribution program for S2 (Fig. 10) shows a tightly defined peak, which again suggests that the sample was reset on deposition. Due to the general lack of coarse-grained alluvium (Fig. 5), the graben infill must postdate the abandonment of the terrace. The lowest parts of the graben infill therefore place a minimum age of the abandonment of the terrace at ~9 +/− 1 ka. This minimum age is not much less than the maximum age of 13 ka determined from sample S5 (taken from 0.7 m below the top surface of the terrace).

In the quarry excavation, the top surface of the scarp is covered by colluvial deposits. The top layer of colluvium is displaced by ~10 cm by a low angle thrust fault (Figs. 6 and 7). Sample S6 is taken from this top layer of colluvium (the sample was taken from only 10 cm below the surface). S6 yields an OSL age of 3 +/− 0.3 ka. Although we cannot be sure that the OSL signal in the colluvial sediments was fully reset on deposition (though the tightly defined peak in the dose distribution diagram, Fig. 10, does suggest resetting), our results do show that the faulting that cuts the sediments must date from the last few thousand years. It is possible that this fault represents surface deformation from the 1052 A.D. Baihaq earthquake, which is likely to have occurred on the Sabzevar fault ([4]; also see Section 2). We cannot however rule out that this earthquake occurred on another nearby fault, or that if it did happen on the Sabzevar fault, that it failed to break the surface, and that we are instead seeing an earlier event.

We can use the amount of deformation of the terrace surface in Section 3 to estimate the Holocene uplift rate across the fault. An average of 9.5 m of uplift in the last 9–13 ka gives an uplift rate of ~0.7 to 1 mm/yr. Assuming that the Sabzevar fault at depth is steep, and dips at ~60° N (see Section 3), we can estimate a rate of convergence across the Sabzevar fault of ~0.4–06 mm/yr and a slip-rate of 0.8–1.2 mm/yr. If the Sabzevar fault has a dip of less than 60°, the rate of shortening and fault slip will be higher. For instance, if the fault dips at only 30° (the maximum observed in Fig. 6), the rate of convergence will be 1.3–1.8 mm/yr, and the rate of slip will be in the range 1.5–2.1 mm/yr.

Measurements of slip-rate can be used to estimate the average interval between large earthquakes on the Sabzevar fault, assuming that the entire fault fails in one earthquake. The main segment of the Sabzevar thrust is at least 60 km long (Fig. 1). The magnitude of slip (u) in an earthquake is related to the rupture length (L) by the relationship $u/L \sim 5$ times 10^{-5} [29]. Following this relationship, an earthquake that ruptured the entire fault segment would involve slip of ~3 m. At the slip-rate of ~1 mm/yr determined from our OSL measurements and using a fault dip of 60°, large earthquakes would be expected on average every 3000 years. If the fault dip is less than 60°, the interval between large earthquakes decreases.

6. Conclusions

The results of our study provide one of the first quantitative estimates of slip-rate across an active fault in Iran. Optically stimulated luminescence dating is typically applied to fine-grained loess deposits, where complete re-setting of the signal on deposition can be reliably assumed. However, in many tectonically active parts of the Earth, such sediments are rare and are not exposed in locations suitable for the study of active faults. Our results show that careful site description and interpretation can overcome some of the problems encountered in OSL dating of coarse alluvial sediments. The reliable measurement of fault slip-rates, and of the average intervals between large events, is an important step in assessing seismic hazard as well as for understanding the regional tectonics, especially in regions such as Iran, where earthquakes are a major problem that lead to regular and widespread loss of life.

Acknowledgement

This study would have been impossible without financial assistance from the Royal Society of London in the form of an award (2004/R3-RW) to MF and RTW. The Research Department of Tehran University provided part of the travel expenses for MF to do this project. The School of Geography and Environment of Oxford University has provided all the luminescence experimental facilities and requirements. MF would like to thank Chantal Tribolo, Tom Stevens and Sallie Burrough for their help in the luminescence lab, and G. Duller for the use of his Analyst software. Logistical

help was provided by the Geological Survey of Iran and we thank them for their continued support of our work in Iran. The sample site was originally identified with the help of Hamid Nazari, and was preserved with the assistance of the governor of Sabzevar. We especially thank Reza Tajik and Asghar Dolati for their enthusiastic GPS profiling. Mr. Haqi and Ali were excellent drivers in the field. Two anonymous reviewers are thanked for their constructive comments. RTW is supported by NERC and the NERC-funded Centre for the Observation and Modelling of Earthquakes and Tectonics (COMET).

References

[1] M. Berberian, Earthquake faulting and bedding thrust associated with the Tabas-e-Golshan (Iran) earthquake of September 16, 1978, Bull. Seismol. Soc. Am. 69 (1979) 1861–1887.

[2] M. Berberian, M. Qorashi, J. Jackson, K. Priestley, T. Wallace, The Rudbar-Tarom earthquake of 20 June 1990 in NW Persia: preliminary field and seismological observations, and its tectonic significance, Bull. Seismol. Soc. Am. 82 (1992) 1726–1755.

[3] M. Talebian, E.J. Fielding, G.J. Funning, J. Jackson, H. Nazari, B. Parsons, K. Priestley, M. Ghorashi, P.A. Rosen, R. Walker, T.J. Wright, The 2003 Bam (Iran) earthquake-rupture of a blind strike-slip fault, Geophys. Res. Lett. 31 (2004) L11611, doi:10.1029/2004GL020058.

[4] N.N. Ambraseys, C.P. Melville, A history of Persian earthquakes, Cambridge University Press, U.K., 1982

[5] M. Berberian, R.S. Yeats, Patterns of historical earthquake rupture in the Iranian plateau, Geophys. Res. Lett. 89 (1999) 120–139.

[6] V. Regard, O. Bellier, J.-C. Thomas, D. Bourles, S. Bonnet, M.R. Abbassi, R. Braucher, J. Mercier, E. Shabanian, Sh. Soleymani, Kh. Feghhi, Cumulative right-lateral fault slip-rate across the Zagros–Makran transfer zone: role of the Minab-Zendan fault system in accommodating Arabia–Eurasia convergence in southeast Iran, Geophys. J. Int. 162 (2005) 177–203.

[7] Ph. Vernant, F. Nilfroushan, D. Hatzfeld, M.R. Abbassi, C. Vigny, F. Masson, H. Nanakali, J. Martinod, A. Ashtiani, R. Bayer, F. Tavakoli, J. Chery, Contemporary crustal deformation and plate kinematics in Middle East constrained by GPS measurements in Iran and northern Oman, Geophys. J. Int. 157 (2004) 381–398.

[8] Geological Survey of Iran, Geological Quadrangle map of Iran, Sheet J-4 (Sabzevar), 1:250,000 scale. 1993.

[9] J.P. Avouac, P. Tapponnier, M. Bai, H. You, G. Wang, Active thrusting and folding along the northern Tien Shan and Late Cenozoic rotation of the Tarim relative to Dzungaria and Kazakhstan, J. Geophys. Res. 98 (1993) 6755–6804.

[10] G. Yielding, J.A. Jackson, G.C.P. King, H. Sinvhal, C. Vita-Finzi, R.M. Wood, Relations between surface deformation, fault geometry, seismicity, and rupture characteristics during the El Asnam (Algeria) earthquake of 10 October 1980, Earth Planet. Sci. Lett. 56 (1981) 287–304.

[11] R. Walker, J. Jackson, C. Baker, Thrust faulting in eastern Iran: source parameters and surface deformation of the 1978 Tabas and 1968 Ferdows earthquake sequences, Geophys. J. Int. 152 (2003) 749–765.

[12] L.B.E. Bøtter-Jensen, G.A.T. Duller, A.S. Murray, Advances in luminescence instrument systems, Radiat. Meas. 32 (5–6) (2000) 523–528.

[13] A.S. Murray, A.G. Wintle, Luminescence dating of quartz using an improved single-aliquot regenerative-dose protocol, Radiat. Meas. 32 (1) (2000) 57–73.

[14] s. Stokes, A.E.L. Colls, M. Fattahi, J. Rich, Investigations of the performance of quartz single aliquot DE determination procedures, Radiat. Meas. 32 (5–6) (2000) 585–594.

[15] J. Wallinga, A. Murray, A. Wintle, The single aliquot regenerative-dose (SAR) protocol applied to coarse-grain feldspar, Radiat. Meas. 32 (2000) 529–533.

[16] M. Fattahi, Studies on red thermoluminescence and infrared stimulated red luminescence. Unpublished D. Phil. thesis, Oxford University, Oxford. 2001.

[17] M. Auclairm, M. Lamothe, S. Huot, Measurement of anomalous fading for feldspar IRSL using SAR, Radiat. Meas. 37 (4–5) (2003) 487–492.

[18] G.A.T. Duller, Recent developments in luminescence dating of Quaternary sediments, Prog. Phys. Geogr. 20 (2) (1996) 127–145.

[19] S. Stokes, The timing of OSL sensitivity changes in a natural quartz, Radiat. Meas. 23 (1994) 601–605.

[20] G.A.T. Duller, Equivalent dose determination using single aliquots, Nucl. Tracks Radiat. Meas. 18 (1991) 371–378.

[21] C.A. Richardson, Effects of bleaching on the sensitivity to dose of the infra-red stimulated luminescence of potassium-rich feldspars from Ynyslas, Wales, Nucl. Tracks Radiat. Meas. 18 (1994) 101–107.

[22] S.J. Armitage, R.M. Bailey, The measured dependence of laboratory beta dose rates on sample grain size, Radiat. Meas. 39 (2005) 123–127.

[23] M. Fattahi, R. Walker, Use of optically stimulated luminescence (OSL) in measuring averaged fault slip rates in Iran (in preparation). 2005.

[24] M.J. Aitken, Thermoluminescence Dating, Academic Press, London, 1985.

[25] W.T. Bell, Alpha dose attenuation in quartz grains for thermoluminescence dating, Ancient TL 12 (1980) 4–8.

[26] V. Mejdahl, Thermoluminescence dating: beta-dose attenuation in quartz grains, Archaeometry 21 (1979) 61–72.

[27] J.R. Prescott, G.B. Robertson, Sediments dating by luminescence: a review, Radiat. Meas. 27 (5/6) (1997) 893–922.

[28] S.L. Forman, J. Pierson, K. Lepper, Luminescence geochronology, in: J.S. Noller, J.M. Sowers, W.R. Lettis (Eds.), Quaternary Geochronology — Methods and Applications, AGU Reference Shelf, vol. 4, American Geophysical Union, Washington, DC, 2000, pp. 157–176.

[29] C.H. Scholz, Scaling laws for large earthquakes: consequences for physical models, Bull. Seismol. Soc. Am. 72 (1982) 1–14.